Effect of Oxygen Exchange between Two Oxide Layers of a Memristive Bilayer Valence-Change Memory Cell on the Switching Polarity

Nils Sommer,* Regina Dittmann, and Stephan Menzel†
Peter Grünberg Institute 7, Research Center Jülich, Jülich 52425, Federal Republic of Germany

(Received 21 October 2022; revised 17 February 2023; accepted 23 March 2023; published 26 April 2023)

Valence-change memory (VCM) cells are promising candidates for future nonvolatile memory devices. A special setup of VCM devices consists of bilayer cells where two thin oxide layers are placed in between two metal electrodes. One oxide layer serves as a tunnel barrier, whereas the second oxide layer is a highly doped conductive semiconductor. Experiments show that an exchange of oxygen between the two layers changes the resistance of the cell. However, the exchange process and how it influences the resistance is not well understood yet. With a drift-diffusion model for electrons and oxygen vacancies, we investigate the movement and exchange of oxygen vacancies and their influence on the band structure as well as on the shape of the tunnel barrier. The simulation results show that a high oxygen-vacancy concentration lowers the height of the tunnel barrier; thus it increases the conductivity of the bilayer cell. The effect of the band lowering is stronger in materials with low permittivity. Hence, two different resistance states evolve if there is an exchange of oxygen between the two oxide layers with different permittivities. Thereby, the switching polarity depends on the relation of the permittivities of the two oxide layers. Furthermore, it is revealed that resistance switching can be induced by the movement of vacancies only inside the conductive oxide, without any oxygen exchange between the layers.

DOI: 10.1103/PhysRevApplied.19.044084

I. INTRODUCTION

Memristive switching devices are currently the subject of particular interest in semiconductor research [1,2]. The ability to change their resistance between at least two stable resistance states by applying a bias voltage makes them promising candidates for future memory devices [3] and applications such as in-memory computing [4,5] or neuromorphic computing [6].

It has been shown that the movement of oxygen ions inside an oxide semiconductor can change the resistance of a so-called valence-change memory (VCM) memristor [7]. The oxygen ions can either move as negatively charged oxygen interstitials or by hopping into oxygen-vacancy defects, described as a movement of the positively charged oxygen vacancies [8]. Thereby, the local accumulation of oxygen vacancies changes the resistance of the cell [9–11] by creating conductive paths inside the semiconductor [2,12,13] or by deforming the shape of a Schottky barrier [14–16] at the interface between the oxide semiconductor and an attached electrode. In addition, it has been shown that an exchange of oxygen between materials, e.g., between the oxide semiconductor and a metal electrode, has a significant influence on the behavior of the resistance change [17,18].

One form of behavior that is of particular interest is the switching polarity. For this, a SET process is defined, where the device resistance changes from a high resistive state (HRS) to a low resistive state (LRS), and a RESET process is also defined, where the resistance changes from a LRS to a HRS. Considering that the SET process happens for a positive voltage applied to the so-called active electrode (AE) and the RESET happens for a negative applied voltage, the plotted J-V curve looks like a lying figure eight, which is why this polarity is called eight-wise (8w) switching. If the RESET occurs for positive applied voltages and the SET for negative ones, the polarity is called counter-eight-wise (c8w). Different behaviors of the oxygen ions, e.g., movement only in the oxide or an oxygen exchange with other materials, can result in different switching polarities. Thus, the polarity can indicate which process causes the switching [7].

In this work, we focus on bilayer VCM cells consisting of two oxides placed in between two metal electrodes. One of the oxides serves as a highly resistive thin tunneling barrier for electrons, while the other oxide is a highly doped conductive semiconductor. The tunneling oxide is in contact with a high-work-function metal called the active electrode (AE), creating a high Schottky barrier. The other oxide is in contact with a low-work-function metal; thus the contact shows an Ohmic conducting behavior. This electrode is named the Ohmic electrode (OE). In experiments, it has been observed that some of these

*n.sommer@fz-juelich.de
†st.menzel@fz-juelich.de

bilayer VCM cells show a very gradual change of resistance under an applied voltage and that the resistance changes linearly with the device area [19,20]. This indicates a symmetric process that takes place over the entire device area. Measurements identify an exchange of oxygen ions between the two oxide layers during the switching process, which has been proposed as reason for the resistance change [20–23]. An often-mentioned idea in this context is that this variation of the local ion density bends the band structure and deforms the tunnel barrier and thus affects the change of the resistance [20,22,24].

Based on this idea, our approach is to investigate the influence of the oxygen exchange between the two layers by using a drift-diffusion model for ions and electrons [25,26]. To this end, we model the exchange of oxygen by defining two static oxygen-vacancy distributions. If oxygen ions move from one oxide to the other, they leave a higher oxygen-vacancy concentration inside the oxide that they have left and simultaneously decrease the oxygen-vacancy concentration inside the oxide into which they have moved. Depending on the exchange direction, the oxygen-vacancy concentration inside the tunneling oxide is higher than in the conductive oxide or vice versa. We show that the exchange of oxygen results in different resistance states, while the switching polarity depends on how the permittivities of the materials relate to each other. Our results show that the device is in the LRS when there is a high oxygen-vacancy concentration inside the material with the lower permittivity.

Additionally, we perform dynamic simulations with mobile oxygen vacancies. We modify the mobility of the oxygen vacancies inside the tunneling barrier from nearly immobile to a fast mobility by changing the height of the ion-migration barriers. For high migration barriers, the oxygen vacancies only move inside the conductive oxide, while for low migration barriers, they can move from the conductive oxide into the tunneling oxide, i.e., there is an oxygen exchange. By using two oxides with different permittivities, we observe the same dependence of the switching polarity on the permittivities, as in the static simulations.

II. PHYSICAL MODEL

The simulation model consists of a metal-insulator-semiconductor-metal structure. The insulator is a 2-nm-thick oxide with a high band gap and low electron affinity. The semiconductor is 5 nm thick and has a high electron affinity and a high donor doping by oxygen vacancies. The active electrode that is in contact with the insulator has a high work function, building a Schottky contact, while the other electrode has a low work function, building an Ohmic contact. The Ohmic electrode is grounded while the voltage is applied to the active electrode.

Since the bilayer-cell resistance scales linearly with the device area, we assume a homogeneous oxygen-exchange process over the entire interface area. Thus, instead of simulating a three-dimensional layer stack, we simplify our model one-dimensional (1D) geometry from the active to the Ohmic electrode. The oxide-electrode interfaces denote the boundaries of our model. While the interface to the active electrode is the origin of the coordinate system $x_{\mathrm{AE}} = 0$, the interface to the Ohmic electrode is $x_{\mathrm{OE}} = 7$ nm.

Since for bilayer devices, small current densities have been observed [19,20], the heating by the electric current inside the bilayer device is insignificant. Hence, we assume a constant temperature of 293 K.

Internal and applied electric fields deform the band structure of the semiconductors and exert forces on charges, such as electrons and oxygen vacancies. The electric field is

$$E = -\nabla\Phi. \tag{1}$$

Φ is the electrostatic potential, which is derived as a solution of the Poisson equation,

$$\partial_x\left(\epsilon_0\epsilon_r\,\partial_x\Phi\right) = -e\left(N_D - n\right), \tag{2}$$

where ϵ_0 is the absolute vacuum permittivity, ϵ_r is the relative permittivity of the material, e is the elementary charge, N_D is the local donor concentration only given by double-charged oxygen vacancies, $N_D = 2V_{\mathrm{O}}^{\cdot\cdot}$, and n is the local electron concentration. The boundary conditions for the Poisson equation are the negative electrode work functions $\Phi\,(0) = -\Phi_{\mathrm{work\_AE}} + V_{\mathrm{app}}$ and $\Phi\,(x_{\mathrm{OE}}) = -\Phi_{\mathrm{work\_OE}}$. Here, V_{app} is the voltage that is applied to the active electrode.

The dynamics of the electrons are described by the drift-diffusion equation

$$\frac{\partial n}{\partial t} = \frac{1}{e}\partial_x J_n - R = \frac{1}{e}\partial_x\left(-e\mu_n n\partial_x\Phi + eD_n\partial_x n\right) - R, \tag{3}$$

where μ_n is the electron mobility, R is the recombination rate, and D_n is the diffusion coefficient for the electrons related to the electron mobility by the Nernst-Einstein relation, $D_n = \mu_n(k_BT)/e$, with the Boltzmann constant k_B and the temperature T.

For the application of the drift-diffusion equation for such thin layers, a lot of scattering events are necessary; thus the drift-diffusion equation can be derived from the Boltzmann transport equation. Since the modeled semiconductors are assumed to be highly doped by oxygen vacancies, we consider a lot of scattering events with oxygen vacancies as scattering centers [27]. Furthermore, the more ionic-like structure of the modeled oxide semiconductors

leads to a polar system with reduced electron mobility [28–30]. Hence, the drift-diffusion equation is applicable to our assumed oxide semiconductors with thicknesses of a few nanometers.

The electrons have a high mobility compared to the mobility of the oxygen ions. On time scales on which the motion of oxygen vacancies is observable, the electrons have reached an equilibrium state; thus a steady-state condition for the electrons can be assumed: $\partial n/\partial t \approx 0$. With the relation between the electric current generated by electrons and the quasi Fermi level E_{fn},

$$J_n = \mu_n n \partial_x E_{fn}, \tag{4}$$

Eq. (3) simplifies to

$$qR = \partial_x \left(\mu_n n \partial_x E_{fn}\right). \tag{5}$$

The boundary conditions for the quasi Fermi level are the Fermi levels of the electrodes, i.e., for the Ohmic electrode, $E_{fn}(x_{\mathrm{OE}}) = 0$ and at the active electrode, $E_{fn}(0) = -eV_{\mathrm{app}}$.

The tunnel oxide acts as a thin barrier for the electrons. The tunneling current density is calculated by means of the integral of the tunneling probability and the number of tunneling electrons over the energy levels between the minimum E_{min} and maximum E_{max} energies of the conduction-band edge:

$$J_{\mathrm{tun}} = \frac{4\pi e m^*}{h^3} \int_{E_{\mathrm{min}}}^{E_{\mathrm{max}}} TC\,(E)\, N_{\mathrm{sup}}\,(E)\, dE, \tag{6}$$

where m^* is the effective tunneling mass of the electrons and h is Planck's constant. N_{sup} is the supply function comparing the densities of electrons on both sides of the barrier at a given energy level:

$$N_{\mathrm{sup}}(E) = k_B T \ln\left(\frac{1+\exp\left(\frac{E_{F,M}-E}{k_B T}\right)}{1+\exp\left(\frac{E_{fn}-E}{k_B T}\right)}\right), \tag{7}$$

where $E_{F,M}$ is the Fermi level of the metal electrode. The supply function is negative if there is a higher density of electrons inside the semiconductor and it is positive if the density inside the metal is higher.

The transmission coefficient TC denotes the probability that electrons will tunnel through the barrier. It is calculated by a Wentzel-Kramer-Brillouin (WKB) approximation as

$$TC(E) = \exp\left(\frac{-4\pi}{h}\int_{x_a}^{x_b} \sqrt{2m^*\,(E(x)-E)}\, dx\right). \tag{8}$$

In Eq. (8), x_a and x_b denote points on both sides of the barrier at which the energy level of the conduction-band edge is the same, fulfilling the condition $E(x_a) = E(x_b)$.

The dynamics of the oxygen vacancies are described by a second drift-diffusion equation,

$$\frac{\partial V_{\mathrm{O}}^{\cdot\cdot}}{\partial t} = -\partial_x\left(D_{V_{\mathrm{O}}^{\cdot\cdot}}\partial_x V_{\mathrm{O}}^{\cdot\cdot} + \frac{D_{V_{\mathrm{O}}^{\cdot\cdot}} e}{k_B T} V_{\mathrm{O}}^{\cdot\cdot}\partial_x \Phi\right), \tag{9}$$

with

$$D_{V_{\mathrm{O}}^{\cdot\cdot}} = D_{0V_{\mathrm{O}}^{\cdot\cdot}} \exp\left(-W_A/k_B T\right), \tag{10}$$

where $D_{0V_{\mathrm{O}}^{\cdot\cdot}}$ is a diffusion prefactor and W_A is the migration potential for the oxygen vacancies. Later, we vary W_A to change the diffusion coefficient $D_{V_{\mathrm{O}}^{\cdot\cdot}}$; thus the mobility of the oxygen vacancies increases or decreases.

The average concentration of the oxygen vacancies inside the device is constant; thus the flux over the boundaries at the oxide-metal interfaces is zero. We assume that both materials have the same density of oxygen lattice sites per volume, so that the oxygen-vacancy concentration does not require a correction factor for the dynamic exchange process.

The shape of the conduction band is deformed by the local electric field. The lower edge of the conduction band is calculated by

$$E_c = -\chi - e\Phi, \tag{11}$$

where χ is the electron affinity of the semiconductor.

The local electron concentration is given by a Fermi-Dirac integral of order 1/2,

$$n = N_c F_{1/2}\left(\frac{E_{fn}-E_c}{k_B T}\right), \tag{12}$$

where $N_c = 2\left(2\pi m^* k_B T/h^2\right)^{3/2}$ is the density of states, where h is Planck's constant.

In this simulation study, triangular voltage sweeps with a voltage ramp of 1 V/s and a maximum voltage of ± 3 V are used. The period time of one sweep is 12 s. To investigate the influence of the local vacancy concentration, we perform two types of simulation, i.e., static and dynamic. For the static simulations, we define a time-independent oxygen-vacancy distribution and solve only Eqs. (2) and (5) numerically. For the dynamic simulations, the drift-diffusion equation for oxygen vacancies (9) is also solved. Joule-heating effects are neglected. For all simulations, a constant temperature of $T = 293$K is set.

The material parameters used are listed in Table I. The values are arbitrary but in a range comparable with realistic oxides.

III. SIMULATION AND RESULTS

A. Dependence of the switching polarity on the permittivity of the oxides

In this section, the model focuses on the exchange process between the oxides; thus a small exchange region at

TABLE I. The material parameters used at $T = 293$ K.

Parameter	Tunnel oxide	Conductive oxide
Work function (electrodes)	5.2 eV (AE)	4.0 eV (OE)
Electron affinity χ	2.4 eV	3.8 eV
Electron mobility μ_n	5 cm^2/s	5 cm^2/s
Effective mass m^*	$1m_e$	$1m_e$
Thickness	2 nm	5 nm
Diffusion coefficient $D_{0V_O^{\cdot\cdot}}$	$1 \times 10^{-7} cm^2/s$	$1 \times 10^{-7} cm^2/s$
Variable parameters:		
Relative permittivity ϵ_r	5; 20; 22; 50	20
Migration barrier W_A	0.4; 0.5; 0.6; 0.7 eV	0.5 eV

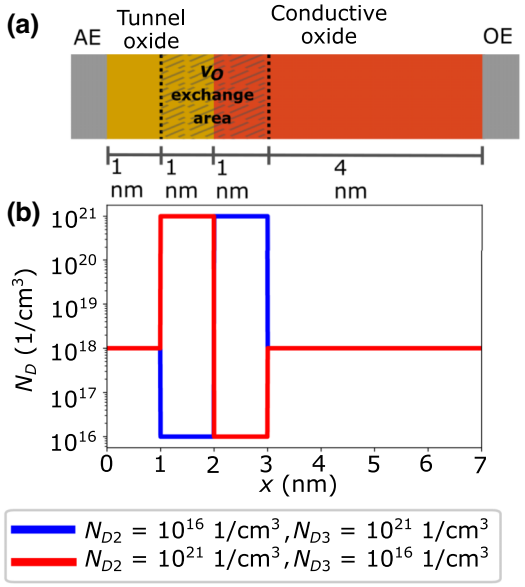

FIG. 1. The oxygen-vacancy distribution for the static simulation. (a) The bilayer composition, with a 2-nm exchange area at the oxide-oxide interface. (b) The two defined oxygen-vacancy distributions. The concentration in the first 1 nm of the tunnel oxide and the last 4 nm of the conductive oxide is the same for both states. Red denotes the state where the oxygen-vacancy concentration inside the tunnel oxide is higher than inside the conductive oxide (after an applied negative voltage). Blue is the inverted state (after applying a positive voltage).

the interface is adopted. It extends from the oxide-oxide interface 1 nm into both oxides. By means of this, the cell is split into four parts: (1) the first 1 nm inside the tunnel oxide, (2) the remaining 1 nm of the tunnel oxide (an exchange region), (3) 1 nm of the conductive oxide (an exchange region), and (4) the remaining 4 nm of the conductive oxide. The four parts are depicted in Fig. 1(a).

We consider an exchange process only, without any ion migration deeper into the oxides. To prevent any influence due to ion motion, we define the successful oxygen exchange between the layers by two static oxygen-vacancy distributions. The first state resembles the configuration after application of a negative voltage pulse. The negative applied voltage attracts the oxygen vacancies toward the active electrode; hence the oxygen vacancies move from the conductive oxide to the tunnel oxide by an exchange of oxygen. Thus, the oxide-oxide interface region of the tunnel oxide is rich in oxygen vacancies while the interface region of the conductive oxide is oxygen vacancy poor. The second state resembles the configuration after a positive voltage is applied. The oxygen vacancies are pushed into the conductive oxide. Thus, the conductive oxide is rich in oxygen vacancies while the tunnel oxide is oxygen vacancy poor.

For all four parts of the bilayer cell, a constant donor concentration, $N_{D1,2,3,4}$, can be defined. Since the vacancy concentration only changes in the exchange region, parts (1) and (4) have a constant donor concentration, which is $N_{D1} = N_{D4} = 1 \times 10^{18}$ cm^{-3}. For the two parts of the exchange region, the donor concentration is $N_D = 1 \times 10^{21}$ cm^{-3} if the part is rich in oxygen vacancies and $N_D = 1 \times 10^{16}$ cm^{-3} if the part is poor in oxygen vacancies. The average donor concentration in exchange regions (2) and (3) is higher compared to regions (1) and (4), since an initial redox reaction during deposition between the two oxides increases the vacancy concentration at the interface [24,31]. The two defined static states are depicted in Ref. 1(b).

Furthermore, the influence of the permittivities of the materials on the switching behavior of the bilayer cell is analyzed. Therefore, three cases are defined: one case where the permittivity of the tunnel oxide is much smaller than the permittivity of the conductive oxide, one where the permittivities are equal, and one where the permittivity of the tunnel oxide is larger. The relative permittivity of the conductive oxide is the same in all three cases, $\epsilon_{r2} = 20$, while the relative permittivity of the tunnel oxide is varied as $\epsilon_{r1} = 5$, $\epsilon_{r1} = 20$, and $\epsilon_{r1} = 50$.

Figure 2 shows the simulation results. Figures 2(a), 2(c), and 2(e) depict the J-V curves for the three cases of different permittivities. Figures 2(b), 2(d), and 2(f) are the corresponding conduction-band edges. The blue lines denote the state after applying a positive voltage and the red lines after applying a negative voltage.

In all figures showing the conduction-band edges [Figs. 2(b), 2(d), and 2(f)], the deformation of the bands by the oxygen vacancies is observable. The high oxygen-vacancy concentration bends down the conduction-band edge. By comparison of the two exchange states (red and blue lines), one can see that the bending is stronger if the

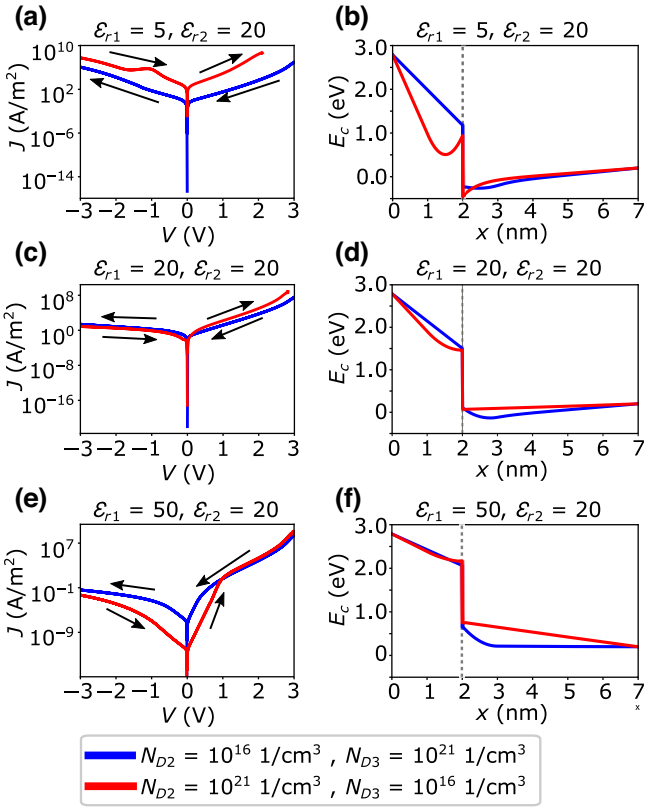

FIG. 2. The dependence of the switching polarity on the relative permittivities of the oxides. The red lines denote states where the vacancy concentration inside the tunnel oxide is higher than in the conductive oxide; the blue lines indicate the inverted state. ϵ_{r1} is the relative permittivity of the tunnel oxide and ϵ_{r2} that of the conductive oxide. (a) The J-V curve for the case where the permittivity of the tunnel oxide is smaller than that of the conductive oxide. The switching polarity is c8w. (c) The case where the permittivities are the same. No switching is observable. (e) The J-V curve for the case where the permittivity of the tunnel oxide is larger than that of the conductive oxide. The switching polarity is 8w. (b),(d),(f) The corresponding conduction-band edges to the J-V curves on the left with no applied voltages ($V_{\text{app}} = 0$ V). One can see that the deformation by the vacancies is stronger inside the oxide with lower permittivity. In (a) and (c), the simulation for the high vacancy concentration inside the tunnel oxide stops at the positive side due to numerical errors.

oxygen vacancies are inside the material with the lower permittivity. Hence, in the case where the permittivity of the tunnel oxide is smaller than the permittivity of the conductive oxide [Figs. 2(a) and 2(b)], the tunneling barrier is lowered more strongly if the oxygen vacancies are inside the tunnel oxide. Due to the lower barrier, the tunneling current is higher. Hence, this case denotes the LRS. The SET to the LRS happens for negative applied voltages, while the RESET happens for positive applied voltages. This switching polarity is c8w.

Figures 2(e) and 2(f) show the opposite case, in which the permittivity of the tunnel oxide is larger than the permittivity of the conductive oxide. In this case, the influence of the oxygen vacancies on the band bending is stronger if the vacancies are inside the conductive oxide (blue line). Compared to the previously discussed case [Figs. 2(a) and 2(b)], the deformation of the tunneling barrier is small. Hence, the deformation of the barrier does not increase the conductivity of the cell. But the higher electron concentration near the interface inside the conductive oxide increases the tunneling current due to the band lowering due to the oxygen vacancies. The SET to the LRS happens for positive applied voltages and the RESET for negative applied voltages. The switching polarity is 8w and, thus, it is inverted compared to the previously discussed case.

The case in which both oxide materials have the same permittivities is shown in Figs. 2(c) and 2(d). If there is a high oxygen-vacancy concentration inside the tunnel oxide, the barrier height is lowered, whereas the conduction-band edge on the side of the conductive oxide near the interface is lowered if the oxygen-vacancy concentration inside the conductive oxide is high. Thus, the electron concentration near this interfaces increases. In Fig. 2(c), it can be seen that there is a kind of RESET for negative and positive applied voltages. Stable LRS and HRS states cannot be defined and there is also no switching polarity.

B. Dynamic movement of oxygen vacancies

In this section, the dynamic case, where the oxygen vacancies are mobile under forces of electric fields and concentration gradients, is investigated. For the simulations, the same bilayer composition is used as for the static simulations. To observe switching, the two oxide layers have different permittivities, where the permittivity of the tunnel oxide is, at $\epsilon_{r1} = 22$, slightly higher than the permittivity of the conductive oxide, $\epsilon_{r2} = 20$. As in the previous section, simulations with the same permittivities could not be performed due to numerical instabilities.

For the dynamics of the oxygen vacancies, a diffusion prefactor of $D_{0V_O^{\cdot\cdot}} = 1 \times 10^{-7}\text{cm}^2/\text{s}$ is used. The ion-migration barrier W_A is varied between 0.4 eV and 0.7 eV in the tunnel oxide, while the migration barrier in the conductive oxide is kept constant at 0.5 eV. The results show that this parameter space provides nearly immobile vacancies for a migration barrier of $W_A = 0.7\,\text{eV}$ and fast mobile vacancies for a migration barrier of $W_A = 0.4\,\text{eV}$. As the initial configuration, a donor concentration of $N_D = 1 \times 10^{16}\text{cm}^{-3}$ in the tunneling oxide and a donor concentration of $N_D = 1 \times 10^{20}\text{cm}^{-3}$ in the conductive oxide are used.

Figure 3 shows the results of the dynamic simulation. For a migration barrier inside the tunnel oxide of 0.7 eV, the ion movement is very slow. Thus, the oxygen-vacancy distribution does not change on the observed time scale

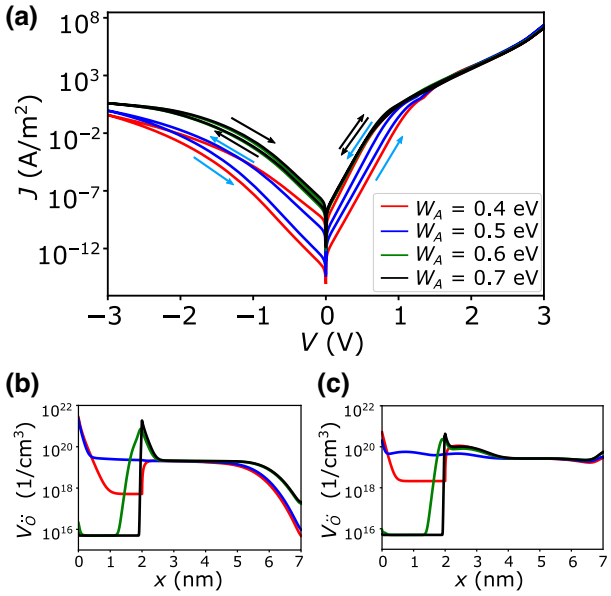

FIG. 3. The switching of the device conductivity by moving oxygen vacancies for different ion-migration barriers inside the tunnel oxide. (a) The J-V curves for different migration barriers inside the tunnel oxide. It shows a change of the switching polarity from 8w polarity for high migration barriers to a c8w polarity for small migration barriers. (b) The vacancy distribution after a negative voltage is applied. For high migration barriers, the oxygen vacancies accumulate at the oxide-oxide interface, while for low barriers, the oxygen vacancies move into the tunnel oxide. (c) The oxygen-vacancy distribution after a positive voltage is applied. The oxygen vacancies are pushed toward the Ohmic electrode.

of a few seconds. Inside the conductive oxide, with a migration barrier of 0.5 eV, a movement of oxygen vacancies (Figs. 3(b) and 3(c) black line) can be observed. Negative applied voltages attract the oxygen vacancies to the oxide-oxide interface, where they accumulate because they cannot migrate into the tunnel oxide due to the high migration barrier inside the tunnel oxide. The accumulation of oxygen vacancies at the interface deforms the tunnel barrier and lowers the conduction-band edge. This leads to a decrease of the device resistance. Positive applied voltages push the oxygen vacancies back toward the Ohmic electrode, which minimizes their effect on the barrier deformation and increases the resistance of the cell. The switching polarity is c8w.

For the case of a migration barrier of 0.6 eV, we observe a small oxygen exchange at the oxide-oxide interface. The difference between the HRS and the LRS is smaller than for the 0.7-eV migration barrier case but the switching polarity is still c8w.

For low migration barriers of 0.5 eV and 0.4 eV, the oxygen vacancies migrate from the conductive oxide into the tunnel oxide when a negative voltage is applied. In this case, there is an oxygen exchange and the switching polarity changes to 8w.

The results match those of the previous static simulation. For negative applied voltages, the oxygen vacancies move toward the tunneling barrier and one expects a SET process to the LRS due to the deformation of the barrier. However, for low migration barriers inside the tunneling oxides, i.e., where an oxygen exchange occurs, a RESET process to the HRS is observed. This can be explained by the different permittivities of the materials. Since the permittivity of the tunneling oxide of $\epsilon_{r1} = 22$ is higher than that of the conductive oxide with $\epsilon_{r2} = 20$, the oxygen vacancies have a lower influence on the barrier deformation if they exchange from the conductive oxide into the tunneling oxide. The change in polarity caused by the occurrence or nonexistence of an oxygen exchange is clearly seen in the J-V curves [Fig. 3(a)]. One difference compared to our static model is that the vacancies now move deep into the oxides and especially to the active electrode. However, this has no influence on the expected switching polarity.

IV. CONCLUSIONS

We investigate the influence of oxygen vacancies on the conduction-band deformation in an n-type bilayer VCM cell. We show that a high oxygen-vacancy concentration deforms the conduction-band edge and can lower the tunnel barrier and thereby effects a change of the cell resistance. The strength of the deformation is stronger in materials with low permittivity. Thus, in a bilayer cell with materials having different permittivities, an exchange of oxygen causes a change of the cell resistance. The switching polarity depends on how the material permittivities relate to each other. Furthermore, we observe another switching process where the vacancies only move inside the conductive oxide and accumulate at the oxide-oxide interface. We show that the polarity of the switching depends on whether the vacancies only move inside the conductive oxide or there is an exchange between the layers.

Assuming that the exchange, and the related deformation of the barrier, is the only reason for the resistive change, our results define a switching polarity for bilayer VCM cells. There are several experiments that have been performed on VCM cells consisting of two oxide layers. Baeumer *et al.* [22] have proposed an area-type switching by an oxygen exchange in their Pt/HfO_2/TaO_x/Ta stack. They have observed a SET process if a negative voltage is applied to the Pt electrode, which indicates a c8w switching. With a permittivity of $\epsilon_r = 25$ for HfO_2, which is slightly higher than for TaO_x with $\epsilon_r = 22$ [32], we would predict a RESET process to occur, contrary to the observed behavior. In the other experiment, Stecconi *et al.* [33] have observed an 8w switching for their Pt/HfO_2/TaO_x/TiN stacks if the voltage is applied to the Pt electrode, which fits with our predictions. Stecconi *et al.* have suggested that their device shows filamentary switching, whereas

our model is developed for area-type devices. While filamentary switching will certainly show different amount of Joule heating due to the largely different current densities, the influence of the distribution of the mobile oxygen ions on the band deformation is similar to that in area-type switching cells as long as a 1D approximation holds. Therefore, we assume that our polarity predictions are also valid for filamentary switching of bilayer VCM cells. Furthermore, the tunneling barrier in the work of Stecconi *et al.* originates at the oxide-oxide interface and not directly at the electrode. Thus, the tunneling barrier is restricted to the emerging thin space-charge region rather than to the total tunneling-oxide thickness. Thus, the physics of the deformation by oxygen vacancies of this tunneling barrier are comparable to our model.

For the case with mobile oxygen ions in only one oxide, Woo *et al.* [31] and Wang *et al.* [34] have both measured the switching behavior of a $TiN/HfO_2/AlO_x$ bilayer device where the AlO_x serves as the tunneling barrier. Woo *et al.* use an aluminum and Wang *et al.* a tungsten electrode on top of the AlO_x. Both argue that the oxygen ion mobility inside the HfO_2 is higher than in AlO_x, so the oxygen vacancies accumulate at the oxide-oxide interface if a negative voltage is applied at the tungsten or aluminum electrode, respectively. In this case, our model predicts a reduction of the barrier height and a decrease in the device resistance; thus the polarity will be c8w. Woo *et al.* observe a c8w switching considering that the voltage is applied to the aluminum electrode, while Wang *et al.* observe an 8w switching. This suggests that although the systems are almost the same, different processes may be taking place. In particular, compared to our model, the movement of oxygen ions in one oxide is not always enough to explain the switching.

Seong *et al.* [21], Assanuma *et al.* [24], and Gutsche *et al*. [19] have observed gradual switching in bilayer devices consisting of $Pr_xCa_{1-x}MnO_2$ (PCMO) with different oxide materials on top, serving as tunneling barriers. Since PCMO is a *p*-type semiconductor, oxygen vacancies as donors will increase the barrier; thus the influence of oxygen vacancies is the opposite to our *n*-type simulation results, e.g., the LRS is reached if the oxygen vacancies are inside the material with the higher permittivity. While Gutsche and Seong have used insulating oxides with a small relative permittivity of $\epsilon_r < 22$ (AlO_x and TaO_x) [32] and observed 8w switching, Assanuma has used TiO_x, an insulator with a high permittivity $\epsilon_r > 80$ [32,35,36], and observed c8w switching. Assuming that the PCMO used has a permittivity somewhere between the permittivities of AlO_x and TaO_x on the one hand and TiO_x on the other, our model also yields different switching polarities but for each experiment individually, our predicted polarity is the opposite of the experimentally observed polarity. However, the thicknesses of the metal oxides range from 4 to 10 nm, which is too thick for electrons to tunnel directly through. For cells with these insulator thicknesses, further current-transport equations are needed, such as trap-assisted tunneling.

To conclude, we compare our predictions to measurements on bilayer VCM cells. Based on our results, we conclude that barrier deformation by an oxygen exchange, as proposed in several works, cannot explain the observed resistance change in all respects. In particular, the possible influence of the oxide permittivities has not been considered so far. Further additional mechanisms need to be taken into account to achieve a full understanding of the switching mechanism.

ACKNOWLEDGMENTS

This work was supported by the Federal Ministry of Education and Research within the Neurotec II project (Project No. 16ME0398K), by the German Research Foundation (Deutsche Forschungsgemeinschaft, DFG) within the SFB917 Nanoswitches, and by the Jülich Aachen Research Alliance (JARA FIT).

[1] J. J. Yang, D. B. Strukov, and D. R. Stewart, Memristive devices for computing, Nat. Nanotechnol. **8**, 13 (2013).
[2] R. Waser, R. Dittmann, G. Staikov, and K. Szot, Redox-based resistive switching memories—nanoionic mechanisms, prospects, and challenges, Adv. Mater. **21**, 2632 (2009).
[3] R. Waser and M. Aono, Nanoionics-based resistive switching memories, Nat. Mater. **6**, 833 (2007).
[4] M. Le Gallo, A. Sebastian, R. Mathis, M. Manica, H. Giefers, T. Tuma, C. Bekas, A. Curioni, and E. Eleftheriou, Mixed-precision in-memory computing, Nat. Electron. **1**, 246 (2018).
[5] D. Ielmini and H.-S. Philip Wong, In-memory computing with resistive switching devices, Nat. Electron. **1**, 333 (2018).
[6] G. Indiveri1, B. Linares-Barranco, R. Legenstein, G. Deligeorgis, and T. Prodromakis, Integration of nanoscale memristor synapses in neuromorphic computing architectures, Nanotechnology **24**, 384010 (2013).
[7] R. Dittmann, S. Menzel, and R. Waser, Nanoionic memristive phenomena in metal oxides: The valence change mechanism, Adv. Phys. **70**, 155 (2021).
[8] A. F. Zurhelle, W. Stehling, R. Waser, R. A. De Souza, and S. Menzel, Oxygen diffusion in platinum electrodes: A molecular dynamics study of the role of extended defects, Adv. Mater. Interfaces **9**, 2101257 (2022).
[9] Y. B. Nian, J. Strozier, N. J. Wu, X. Chen, and A. Ignatiev, Evidence for an Oxygen Diffusion Model for the Electric Pulse Induced Resistance Change Effect in Transition-Metal Oxides, Phys. Rev. Lett. **98**, 146403 (2007).
[10] X. Chen, N. J. Wu, J. Strozier, and A. Ignatiev, Direct resistance profile for an electrical pulse induced resistance change device, Appl. Phys. Lett. **87**, 233506 (2005).

[11] S. H. Jeon, B. H. Park, J. Lee, B. Lee, and S. Han, First-principles modeling of resistance switching in perovskite oxide material, Appl. Phys. Lett. **89**, 042904 (2006).

[12] A. Marchewka, B. Roesgen, K. Skaja, H. Du, C.-L. Jia, J. Mayer, V. Rana, R. Waser, and S. Menzel, Nanoionic resistive switching memories: On the physical nature of the dynamic reset process, Adv. Electron. Mater. **2**, 1500233 (2016).

[13] A. A. Sharma, M. Noman, M. Abdelmoula, M. Skowronski, and J. A. Bain, Electronic instabilities leading to electroformation of binary metal oxide-based resistive switches, Adv. Funct. Mater. **24**, 5522 (2014).

[14] A. Sawa, T. Fujii, M. Kawasaki, and Y. Tokura, Hysteretic current-voltage characteristics and resistance switching at a rectifying $Ti/Pr_{0.7}Ca_{0.3}MnO_3$ interface, Appl. Phys. Lett. **85**, 4073 (2004).

[15] D. J. Seong, M. Jo, D. Lee, and H. Hwang, Hpha effect on reversible resistive switching of Pt/Nb-doped $SrTiO_3$ Schottky junction for nonvolatile memory application, Electrochem. Solid State Lett. **10**, H168 (2007).

[16] C.-W. Hsu, Y.-F. Wang, C.-C. Wan, I-T. Wang, C.-T. Chou, W.-L. Lai, Y.-J. Lee, and T.-H. Hou, Homogeneous barrier modulation of TaO_x/TiO_2 bilayers for ultra-high endurance three-dimensional storage-class memory, Nanotechnology **25**, 165202 (2014).

[17] D. Cooper, C. Baeumer, N. Bernier, A. Marchewka, C. La Torre, R. E. Dunin-Borkowski, S. Menzel, R. Waser, and R. Dittmann, Anomalous resistance hysteresis in oxide ReRAM: Oxygen evolution and reincorporation revealed by in situ TEM, Adv. Mater. **29**, 1700212 (2017).

[18] H. Zhang, S. Yoo, S. Menzel, C. Funck, F. Cüppers, D. J. Wouters, C. S. Hwang, R. Waser, and S. Hoffmann-Eifert, Understanding the coexistence of two bipolar resistive switching modes with opposite polarity in $Pt/TiO_2/Ti/Pt$ nanosized ReRAM devices, ACS Appl. Mater. Interfaces **10**, 29766 (2018), PMID: 30088755.

[19] A. Gutsche, S. Siegel, J. Zhang, S. Hambsch, and R. Dittmann, Exploring area-dependent $Pr_{0.7}Ca_{0.3}MnO_3$-based memristive devices as synapses in spiking and artificial neural networks, Front. Neurosci. **15**, 661261 (2021).

[20] B. Arndt, F. Borgatti, F. Offi, M. Phillips, P. Parreira, T. Meiners, S. Menzel, K. Skaja, G. Panaccione, D. A. MacLaren, R. Waser, and R. Dittmann, Spectroscopic indications of tunnel barrier charging as the switching mechanism in memristive devices, Adv. Funct. Mater. **27**, 1702282 (2017).

[21] D.-J. Seong, M. Hassan, H. Choi, J. Lee, J. Yoon, J.-B. Park, W. Lee, M.-S. Oh, and H. Hwang, Reistive-switching characteristics of $Al/Pr_{0.7}Ca_{0.3}MnO_3$ for nonvolatile memory applications, IEEE Electron Device Lett. **30**, 919 (2009).

[22] C. Baeumer, T. Heisig, B. Arndt, K. Skaja, F. Borgatti, F. Offi, F. Motti, G. Panaccione, R. Waser, S. Menzel, and R. Dittmann, Spectroscopic elucidation of ionic motion processes in tunnel oxide-based memristive devices, Faraday Discuss. **213**, 215 (2019).

[23] C.-Y. Huang, C.-Y. Huang, T.-L. Tsai, C.-A. Lin, and T.-Y. Tseng, Switching mechanism of double forming process phenomenon in ZrO_x/HfO_y bilayer resistive switching memory structure with large endurance, Appl. Phys. Lett. **104**, 062901 (2014).

[24] S. Asanuma, H. Akoh, H. Yamada, and A. Sawa, Relationship between resistive switching characteristics and band diagrams of $Ti/Pr_{1-x}Ca_xMnO_3$ junctions, Phys. Rev. B **80**, 235113 (2009).

[25] V. Saraswat, S. Prasad, A. Khanna, A. Wagh, A. Bhat, N. Panwar, S. Lashkare, and U. Ganguly, Reaction-drift model for switching transients in $Pr_{0.7}Ca_{0.3}MnO_3$ resistive RAM, IEEE Trans. Electron Devices **67**, 3610 (2020).

[26] D. B. Strukov, J. L. Borghetti, and R. S. Williams, Coupled ionic and electronic transport model of thin-film semiconductor memristive behavior, Small **5**, 1058 (2009).

[27] T. Markussen, R. Rurali, A.-P. Jauho, and M. Brandbyge, Scaling Theory Put into Practice: First-Principles Modeling of Transport in Doped Silicon Nanowires, Phys. Rev. Lett. **99**, 076803 (2007).

[28] H. P. R. Frederikse, W. R. Thurber, and W. R. Hosler, Electronic transport in strontium titanate, Phys. Rev. **134**, A442 (1964).

[29] C. Funck, A. Marchewka, C. Bäumer, P. C. Schmidt, P. Müller, R. Dittmann, M. Martin, R. Waser, and S. Menzel, A theoretical and experimental view on the temperature dependence of the electronic conduction through a Schottky barrier in a resistively switching $SrTiO_3$-based memory cell, Adv. Electron. Mater. **4**, 1800062 (2018).

[30] C. Funck, C. Bäumer, S. Wiefels, T. Hennen, R. Waser, S. Hoffmann-Eifert, R. Dittmann, and S. Menzel, Comprehensive model for the electronic transport in $Pt/SrTiO_3$ analog memristive devices, Phys. Rev. B **102**, 035307 (2020).

[31] J. Woo, K. Moon, J. Song, S. Lee, M. Kwak, J. Park, and H. Hwang, Improved synaptic behavior under identical pulses using AlO_x/HfO_2 bilayer RRAM array for neuromorphic systems, IEEE Electron Device Lett. **37**, 994 (2016).

[32] J. Robertson, High dielectric constant oxides, Eur. J. Appl. Phys. **28**, 265 (2004).

[33] T. Stecconi, R. Guido, L. Berchialla, A. La Porta, J. Weiss, Y. Popoff, M. Halter, M. Sousa, F. Horst, D. Dávila, U. Drechsler, R. Dittmann, B. J. Offrein, and V. Bragaglia, Filamentary TaO_x/HfO_2 ReRAM devices for neural networks training with analog in-memory computing, Adv. Electron. Mater. **8**, 2200448 (2022).

[34] Q. Wang, Y. Wang, R. Luo, J. Wang, L. Ji, Z. Jiang, C. Wenger, Z. Song, S. Song, W. Ren, J. Bi, and G. Niu, Ultrathin HfO_2/Al_2O_3 bilayer based reliable 1T1R RRAM electronic synapses with low power consumption for neuromorphic computing, Neuromorphic Comput. Eng. **2**, 044012 (2022).

[35] J. Bonkerud, C. Zimmermann, P. M. Weiser, L. Vines, and E. Minahov, On the permittivity of titanium dioxide, Sci. Rep. **11**, 12443 (2021).

[36] L. Nocolini, A new dielectric material, Nature **170**, 938 (1952).